

Turbo Receiver Design with Joint Detection and Demapping for Coded Differential BPSK in Bursty Impulsive Noise Channels

Chin-Hung Chen, *Student Member, IEEE*, Boris Karanov, *Member, IEEE*,
Wim van Houtum, *Senior Member, IEEE*, Yan Wu, and Alex Alvarado, *Senior Member, IEEE*

Abstract—It has been recognized that the impulsive noise (IN) generated by power devices poses significant challenges to wireless receivers in practice. In this paper, we assess the achievable information rate (AIR) and the performance of practical turbo receiver designs for a well-established Markov-Middleton IN model. We utilize a commonly used commercial transmission setup consisting of a convolutional encoder, bit-level interleaver, and a differential binary phase-shift keying (DBPSK) symbol mapper. Firstly, we conduct a comprehensive assessment of the AIRs of the underlying channel model using DBPSK transmitted symbols across various channel conditions. Additionally, we introduce two robust turbo-like receiver designs. The first design features a separate IN detector and a turbo-demapper-decoder. The second design employs a joint approach, where the extrinsic information of both the detector and demapper is simultaneously updated, forming a turbo-detector-demapper-decoder structure. We show that the joint design consistently outperforms the separate design across all channel conditions, particularly in low AIR situations. However, the maximum performance gain for the channel conditions considered in this paper is merely 0.2 dB, and the joint system incurs significantly greater computational complexity, especially for a high number of turbo iterations. The performance of the two proposed turbo receiver designs is demonstrated to be close to the estimated AIR, with a performance gap dependent on the channel parameters.

Index Terms—Achievable information rate, impulsive noise, Markov channels, symbol detector, turbo decoding.

I. INTRODUCTION

ELECTROMAGNETIC interference (EMI) generated by power devices such as switching gears, power lines, and DC-DC converters presents significant challenges to conventional receivers designed for the additive white Gaussian noise (AWGN). Measurements have shown that electronic components in electric vehicles (EVs) [1]–[4] and power substations [5], [6] emit EMI that can be detected by high-sensitivity receivers. Specifically, the impulsive nature of this interference has been demonstrated to have a crucial impact

on powerline communications [7], [8], digital broadcasting systems [9], [10], and wireless communication receivers within power substations [11]–[13].

To design robust receivers for channels impaired by impulsive noise (IN), it is essential to appropriately model the noise behavior. One of the well-known IN models is the Middleton Class A model [14], [15], which is characterized by a Poisson-distributed IN with a tractable probability density function that can be controlled by only three parameters. Despite its straightforward representation, this model does not adequately describe the bursty behavior of the IN. Therefore, the hidden-Markov model (HMM) has been adopted for IN modeling [8], [16], [17] to address the correlation between impulsive samples. In [16], a two-state Markov-Gaussian model was proposed, where comprehensive achievable information rate (AIR) analysis was presented. In [17], the authors combined the HMM process with the Middleton Class A model and proposed the Markov-Middleton model. In our earlier study [4], we found that a Markov-Middleton model with finite IN states effectively represents the EV-induced interference. However, to the best of our knowledge, an information-theoretical analysis of this model has not been thoroughly investigated; therefore, this paper aims to fill this gap by conducting a detailed AIR analysis under various channel conditions.

Robust receiver design, considering the IN channels, requires a specially designed detector that takes into account the statistical properties of the IN as discussed in [17]–[19]. Moreover, powerful coding systems in combination with the IN detector have been extensively investigated to approach the AIR for the underlying channel model [20]–[26]. Receivers for these coding schemes take the soft information provided by the IN detector and employ iterative decoding algorithms, such as low-density parity-check (LDPC) codes and turbo-like decoders. However, most results in the literature treat the detector and decoder as separate receiver building blocks. There is limited exploration of the joint design where the extrinsic information is exchanged between the IN detector and the decoder. Although in [16] a turbo detector-decoder structure where the LDPC decoder and the IN detector exchange soft information was constructed, the available results are limited to one specific IN channel condition. This paper examines separate and joint turbo detector-decoder designs, evaluating their performance across various channel scenarios. Additionally, we discuss the trade-off between computational complexity and performance improvements.

Manuscript received xx, xxxx; revised xx, xxxx.

C.-H. Chen, W. van Houtum, and A. Alvarado are with the Information and Communication Theory (ICT) Lab, Electrical Engineering Department, Eindhoven University of Technology, 5600MB Eindhoven, The Netherlands. C.-H. Chen and W. van Houtum are also with NXP Semiconductors, High Tech Campus 46, 5656AE Eindhoven, The Netherlands. (*e-mails: c.h.chen@tue.nl; w.j.v.houtum@tue.nl; a.alvarado@tue.nl*).

B. Karanov is with the Communications Engineering Lab (CEL), Karlsruhe Institute of Technology, 76187 Karlsruhe, Germany (*e-mail: boris.karanov@kit.edu*).

Y. Wu is with NXP Semiconductors, High Tech Campus 46, 5656AE Eindhoven, The Netherlands. (*e-mail: yan.wu_2@nxp.com*).

In wireless communication standards such as digital audio broadcasting, terrestrial-Digital Multimedia Broadcasting, and WiFi IEEE 802.11g, the combination of a convolutional encoded and differential phase-shift keying (DPSK) symbol modulator is a popular transmission configuration. In a DPSK system, the symbol is encoded differentially, such that the information is conveyed through the phase difference between each pair of received symbols. Research has demonstrated that a coherent DPSK demapper can be constructed, wherein the soft information output can be computed using the maximum a-posteriori (MAP) rule [27]. Since then, turbo-DPSK systems, which combine a MAP DPSK demapper with a MAP decoder, have been explored in a broad range of literature [28]–[30]. The recursive nature of the DPSK modulator increases the time diversity of a serial turbo-like receiver structure. As a result, a turbo-DPSK system achieves significant performance gains compared to a turbo-PSK receiver, as reported in [31].

Inspired by [16], this paper starts with an information-theoretical analysis of an IN channel and then proposes iterative receiver designs to approach the estimated AIR. Our paper distinguishes itself from [16] by evaluating AIRs and developing robust turbo receivers based on a convolutional coded DPSK transmission format over a Markov-Middleton noise model. We thoroughly analyze the AIR and use the likelihood function to explain its behavior across different channel parameters. Moreover, we propose two practical turbo receiver structures. One is based on a separate detector and turbo-demapper-decoder design. In the other receiver design, we combine the detector and demapper to form a joint system with a turbo-detector-demapper-decoder structure. The joint receiver is shown to outperform the separate design, with the performance gain being particularly prominent under channel conditions characterized by a low AIR. However, a joint design also comes with a higher computational complexity when operating with many turbo iterations. Furthermore, our study shows that the performance of the practical receivers reflects the behavior of the AIR analysis under different channel parameters.

The remainder of this paper is organized as follows: Sec. II presents the general structure and inference algorithm of HMMs. Sec. III introduces the system model and reviews the Markov-Middleton IN channel and its HMM representation. Sec. IV illustrates the simulated AIR for different channel conditions. Sec. V details the design methodology for separate and joint turbo receivers considering the IN statistics. Sec. VI presents the simulation results, and finally, Sec. VII concludes this paper.

II. HIDDEN MARKOV MODEL AND ITS EFFICIENT INFERENCE ALGORITHM

This section provides a general overview of the structure and statistical representation of HMMs. Additionally, we present the utilization of the forward-backward algorithm to compute joint probabilities of observations and latent variables. An HMM structure will be used to describe the Markov-Middleton IN channel in Sec. III-B, and the inference algorithm presented in this section will later be applied to AIR computation,

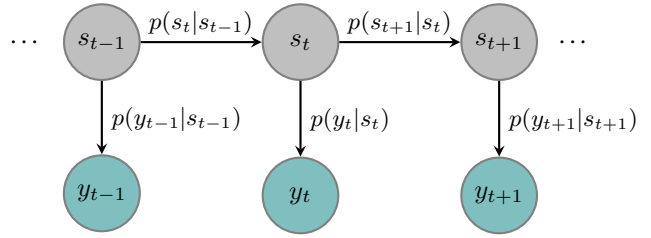


Fig. 1. Structure of a hidden Markov model representation in (1) showing the factorization and conditional independencies implied by the model.

symbol detection, differential demodulation, and convolutional decoding based on the MAP rule. These applications will be further explained in Secs. IV and V.

An HMM is a statistical model that captures the temporal behavior of a sequence of latent variables (states) from a Markov process via a sequence of state-dependent observable variables (observations). In particular, the model represents the joint distribution of the observed sequence $\mathbf{y}_1^T = (y_1, y_2, \dots, y_T)$ and the corresponding state sequence $\mathbf{s}_1^T = (s_1, s_2, \dots, s_T)$ as

$$p(\mathbf{s}_1^T, \mathbf{y}_1^T) = \prod_{t=1}^T p(s_t | s_{t-1}) p(y_t | s_t), \quad (1)$$

where at $t = 1$, the transition probability $p(s_1 | s_0)$ is defined as the initial state probability $p(s_1)$.¹ Here, s_t denotes the actual state realization at time t , which is drawn from a time-invariant finite-state set

$$s_t \in \mathcal{S} = \{0, 1, \dots, |\mathcal{S}| - 1\}, \quad (2)$$

where $|\mathcal{S}| = N$ is the size of the state space. This paper assumes that the state transition matrix is stationary, with each element representing the probability $p(s_t = j | s_{t-1} = i)$ of moving from state i at time $t-1$ to state j at time t . The second parameter on the right-hand side of (1) is the observation likelihood $p(y_t | s_t = j)$, which describes the probability of an observation being generated from a state j at time t . A general representation of the structure of an HMM is shown in Fig. 1.

The Markovian structure of an HMM allows an efficient inference of the hidden states through the well-known Bahl-Cocke-Jelinek-Raviv (BCJR) algorithm [33]. Specifically, the inference problem aims at calculating the posterior belief of a latent state s_t at a specific time instant given the full sequence of observation as

$$p(s_t | \mathbf{y}_1^T) \propto p(s_t, \mathbf{y}_1^T) = \sum_{s_{t-1} \in \mathcal{S}} p(s_t, s_{t-1}, \mathbf{y}_1^T). \quad (3)$$

The right-most side of (3) represents the joint distribution of the state pairs (s_t, s_{t-1}) at a specific time t and the whole

¹Throughout this paper, we use lowercase letters to represent a scalar with subscripts indicating a specific time instant and boldface letters to denote a sequence, with subscripts and superscripts denoting the start and end of the sequence.

received sequence \mathbf{y}_1^T . We can further factorize the joint probability as follows

$$p(s_t, s_{t-1}, \mathbf{y}_1^T) = p(s_t, s_{t-1}, \mathbf{y}_{t+1}^T, y_t, \mathbf{y}_1^{t-1}) \quad (4)$$

$$= p(\mathbf{y}_{t+1}^T | s_t, s_{t-1}, y_t, \mathbf{y}_1^{t-1}) \quad (5)$$

$$\begin{aligned} & \cdot p(y_t, s_t | s_{t-1}, \mathbf{y}_1^{t-1}) \cdot p(s_{t-1}, \mathbf{y}_1^{t-1}) \\ & = \underbrace{p(\mathbf{y}_{t+1}^T | s_t)}_{\beta(s_t)} \cdot \underbrace{p(y_t, s_t | s_{t-1})}_{\gamma(s_t, s_{t-1})} \cdot \underbrace{p(s_{t-1}, \mathbf{y}_1^{t-1})}_{\alpha(s_{t-1})}, \end{aligned} \quad (6)$$

where in (4), we separate the observation sequence into past time sequence \mathbf{y}_1^{t-1} , current time step y_t , and the future time sequence \mathbf{y}_{t+1}^T . From (4) to (5) Bayes' rule is used. The derivation of (6) from (5) is based on the Markovian conditional independencies implied by the graph in Fig. 1. Let $\alpha(s_{t-1})$, $\beta(s_t)$, and $\gamma(s_t, s_{t-1})$ represent $p(s_{t-1}, \mathbf{y}_1^{t-1})$, $p(\mathbf{y}_{t+1}^T | s_t)$, and $p(y_t, s_t | s_{t-1})$, respectively, corresponding to the forward recursion, backward recursion, and branch metrics in (6).

Using Bayes' rule and Markovian property, the branch metric γ can be further derived as

$$\gamma(s_t, s_{t-1}) \triangleq p(y_t, s_t | s_{t-1}) = p(y_t | s_t) \cdot p(s_t | s_{t-1}) \quad (7)$$

which can be seen as the multiplication of the observation likelihood and the state transition probability. The forward recursion representation of α can be derived as

$$\alpha(s_t) \triangleq p(s_t, \mathbf{y}_1^t) = \sum_{s_{t-1} \in \mathcal{S}} p(s_t, s_{t-1}, y_t, \mathbf{y}_1^{t-1}) \quad (8)$$

$$= \sum_{s_{t-1} \in \mathcal{S}} p(y_t, s_t | s_{t-1}) \cdot p(s_{t-1}, \mathbf{y}_1^{t-1}) \quad (9)$$

$$= \sum_{s_{t-1} \in \mathcal{S}} \gamma(s_t, s_{t-1}) \cdot \alpha(s_{t-1}), \quad (10)$$

where in (8) the law of total probability is applied, and from (8) to (9) Bayes' rule and the Markovian property are used. Following a similar approach, we can represent the backward recursion β as

$$\begin{aligned} \beta(s_{t-1}) & \triangleq p(\mathbf{y}_{t+1}^T | s_{t-1}) = \sum_{s_t \in \mathcal{S}} p(s_t, \mathbf{y}_{t+1}^T, y_t | s_{t-1}) \\ & = \sum_{s_t \in \mathcal{S}} p(\mathbf{y}_{t+1}^T | s_t) \cdot p(y_t, s_t | s_{t-1}) \\ & = \sum_{s_t \in \mathcal{S}} \beta(s_t) \cdot \gamma(s_t, s_{t-1}). \end{aligned} \quad (11)$$

The forward-backward computation (3)–(11) of the posterior belief comprises the conventional BCJR algorithm. In this paper, we will examine several adaptations of this algorithm, each utilizing the same forward-backward framework but with modifications to the branch metrics γ that are tailored to specific applications.

III. SYSTEM MODEL

In Fig. 2, we show the overall structure and components of the transmission system over a Markov-Middleton IN channel considered in this paper. This section will first introduce the bit-interleaved convolutional coded DPSK transmitter. Then,

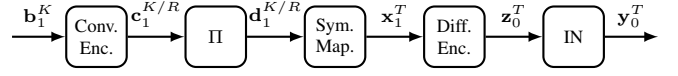


Fig. 2. Block diagram of a convolutionally coded bit-interleaved differential PSK transmission over an impulsive noise channel

we summarize the Markov-Middleton model, initially developed for powerline communications [17], which effectively captures the statistical behavior of bursty noises by combining an HMM process with a truncated Middleton Class A model.

A. Bit-interleaved Convolutional-coded DPSK transmitter

On the transmitter side, a serially concatenated bit-interleaved coded modulation is constructed for transmission. In this system, a rate R convolutional encoder with L -stage shift register takes as input the information bit sequence \mathbf{b}_1^K and generates coded bit sequence output $\mathbf{c}_1^{K/R}$, where $b_k, c_k \in \mathcal{U} = \{0, 1\}$, based on a certain generator constraint. A bit-level interleaver (Π) is used to permute the convolutional encoder output, where the interleaved coded bit sequence is represented as $\mathbf{d}_1^{K/R}$. The bit-interleaver is designed to transform burst errors into single-bit errors that ensure that errors are distributed to maximize error correction capability, which is essential for turbo decoding. After the interleaver, a symbol sequence \mathbf{x}_1^T is formed by a memoryless binary PSK (BPSK) symbol mapper, which maps a number of binary coded bits to a symbol $x_t \in \mathcal{X} = \{+1, -1\}$. The symbol time index is denoted by the letter t . Finally, a differential symbol encoder modulates the incoming BPSK symbols and generates the differentially encoded differential BPSK (DBPSK) symbol sequence \mathbf{z}_0^T by

$$z_t = x_t \cdot z_{t-1}, \quad (12)$$

where we define $z_0 = 1$ and $z_t \in \mathcal{X}$. Differential encoders are used in various wireless communication standards. One of the most significant advantages of a differential encoder is that it avoids the need for the receiver to have an exact phase reference, as the information is encoded in the phase difference of consecutive symbols. In this paper, we treat the differential encoder as a rate one convolutional code [28], [31] and thus create a serial-like turbo structure with the error correction encoder. Its recursive structure largely enhances the time diversity in the serial turbo receiver design, leading to significant performance improvement compared to memoryless PSK modulation schemes [29], [30]. This study assumes a coherent detection scenario with a known symbol phase. As a result, we will ignore the reference symbols z_0 and y_0 in the subsequent analysis.

B. Markov-Middleton Impulsive Noise Model

The Markov-Middleton model was proposed in [17] to describe the bursty IN behavior observed in practice. This model combines the conventional Middleton Class A IN model [14] with HMM to incorporate the memory between the noise samples. More specifically, the inclusion of state transition

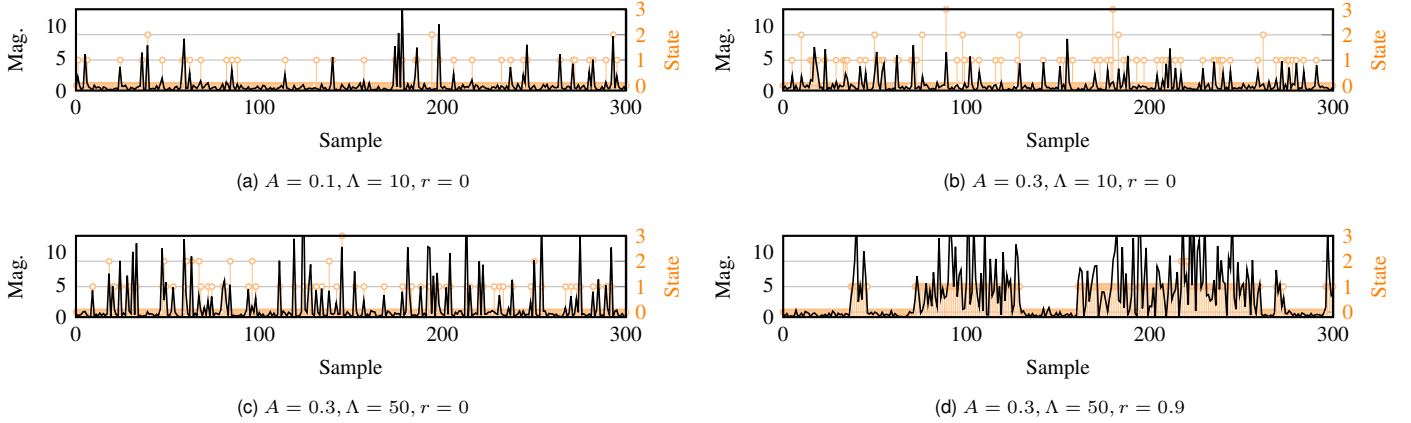


Fig. 3. Noise realization from a 4-state Markov-Middleton impulsive noise model with a background noise variance $\sigma_0^2 = 1$ for impulsive index $A = 0.1$ and $A = 0.3$, impulsive-to-background noise power ratio $\Lambda = 10$ and $\Lambda = 50$, and correlation parameters $r = 0$ and $r = 0.9$. The orange vertical bar denotes the index j of the state realizations $w_t = j$ for generating the corresponding noise samples.

probability describes the correlation property between consecutive noise samples.

The Markov-Middleton model is characterized by four parameters: the background noise (BN) variance σ_0^2 , the impulsive index A , which quantifies the probability of impulsive (non-BN) events, the impulsive-to-background noise power ratio Λ , which determines the intensity of IN compared to BN, and the noise correlation parameter r , which describes the correlation between consecutive noise samples. The noise realizations generated by the Markov-Middleton model for different parameters are depicted in Figs. 3a–3d, and will be further explained in the following.

For transmission over a Markov-Middleton IN channel, the received sample sequence \mathbf{y}_1^T can be described by

$$y_t = z_t + n_t \quad (13)$$

where \mathbf{z}_1^T is the transmitted symbol sequence shown in (12) and \mathbf{n}_1^T represents the noise sample sequence. The noise samples are independent of the transmitted symbols. The statistical properties of n_t are completely determined by the channel noise state realization at time t , which is defined as

$$w_t \in \mathcal{W} = \{0, 1, \dots, |\mathcal{W}| - 1\}, \quad (14)$$

where $w_t = 0$ represents the BN state and $|\mathcal{W}| = W$ is the total number of channel noise states. The probability density function (PDF) of n_t conditioned on a specific noise state $w_t = j$ can be written as

$$p(n_t | w_t = j) = \frac{1}{\sqrt{2\pi\sigma_j^2}} \exp\left(-\frac{n_t^2}{2\sigma_j^2}\right), \quad (15)$$

where σ_j^2 is the variance of the noise sample n_t being at a specific state $w_t = j$.

In the original Middleton Class A model [14], the number of noise states is assumed to be infinity ($W \rightarrow \infty$). Therefore,

the generic PDF of the Middleton Class A noise sample can be written as the expectation over all possible states as

$$\begin{aligned} p(n_t) &= \sum_{j=0}^{\infty} p(w_t = j) \cdot p(n_t | w_t = j) \\ &= \sum_{j=0}^{\infty} \frac{p(w_t = j)}{\sqrt{2\pi\sigma_j^2}} \exp\left(-\frac{n_t^2}{2\sigma_j^2}\right), \end{aligned} \quad (16)$$

where

$$p(w_t = j) = e^{-A} A^j / j! \quad (17)$$

represents the prior probability of being at a specific noise state. From (17), we can observe that when $j = 0$, the probability of being at BN state $w_t = 0$ is $p_B = p(w_t = 0) = e^{-A}$ and the probability of being at any of the impulsive states $j > 0$ is $p_I = 1 - e^{-A}$. In other words, a larger impulsive index A results in a larger p_I , and thus, more noises with large variance (σ_j^2 , $j > 0$) are generated in a noise sequence \mathbf{n}_1^T . As shown in Figs. 3a and 3b, when the impulsive index A is increased from 0.1 to 0.3, the number of noise in IN states ($j > 0$) increases.

As illustrated in (17), the probability of being in the j -th noise state decreases as j increases. Therefore, it is sufficient to use a truncated Middleton Class A model with a finite number of states W to represent the IN channel with

$$p(n_t) = \sum_{j=0}^{W-1} \frac{p'(w_t = j)}{\sqrt{2\pi\sigma_j^2}} \exp\left(-\frac{n_t^2}{2\sigma_j^2}\right), \quad (18)$$

where the probability of being in state j is now written as

$$p'(w_t = j) = \frac{p(w_t = j)}{\sum_{i=0}^{W-1} p(w_t = i)}. \quad (19)$$

The denominator in (19) is a normalization factor to ensure the total probability equals 1.

The noise variance in (18) is defined as

$$\sigma_j^2 = \left(1 + \frac{j\Lambda}{A}\right) \sigma_0^2, \quad (20)$$

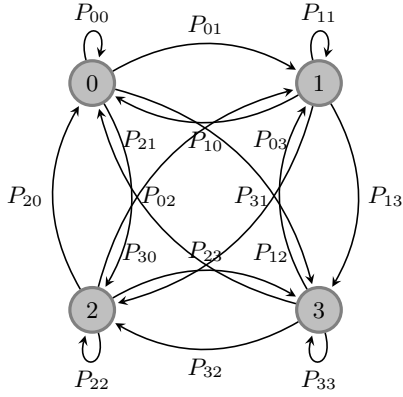


Fig. 4. State diagram representation of a 4-state Markov-Middleton model, where P_{ij} denotes the transition probability from noise state i to state j

where

$$\Lambda = \sigma_I^2 / \sigma_B^2 \quad (21)$$

is the impulsive-to-background average noise power ratio.² The average BN power is $\sigma_B^2 = p'(w_t = 0)\sigma_0^2$ and the average IN power σ_I^2 can be written as

$$\sigma_I^2 = \sum_{j=1}^{W-1} p'(w_t = j)\sigma_j^2.$$

From (21), we can see that as the impulsive-to-background noise ratio Λ increases, the difference between the IN power and the BN power increases. This is clearly shown by comparing the noise realizations (black lines) in Figs. 3b and 3c.

To describe the burstiness (memory) of the noise observed in practice, the Markov-Middleton model [17] introduces a parameter $r \in [0, 1)$ to establish a correlation between consecutive noise samples. Specifically, the state transition matrix of the Markov-Middleton noise model is constructed as

$$P_{ij} = p(w_t = j | w_{t-1} = i) = \begin{cases} r + (1-r) \cdot p'(w_t = j), & i = j \\ (1-r) \cdot p'(w_t = j), & \text{otherwise.} \end{cases} \quad (22)$$

An example of the transition diagram for a 4-state Markov-Middleton model is shown in Fig. 4, where the states are fully connected with the transition probability P_{ij} . From (22), we can see that the larger the correlation parameter r , the more likely the following noise sample will stay in the same state. Namely, the bursty behavior is more prominent. In Fig. 3d, the noise samples exhibit strong correlations ($r = 0.9$), where the noise tends to remain in the same state (vertical orange bars) for consecutive samples. In contrast, in Figs. 3a–3c, the noise samples are randomly chosen from $w_t \in \mathcal{W}$ with probability $p'(w_t = j)$ defined in (19). Note that when $r = 0$, the Markov-Middleton model is reduced to a truncated memoryless Middleton Class A channel.

IV. ACHIEVABLE INFORMATION RATE ANALYSIS

This section presents an information-theoretical analysis of the Markov-Middleton IN model introduced in Sec. III-B.

²In the original paper [14], the power ratio is defined as $\Gamma = \sigma_B^2 / \sigma_I^2$.

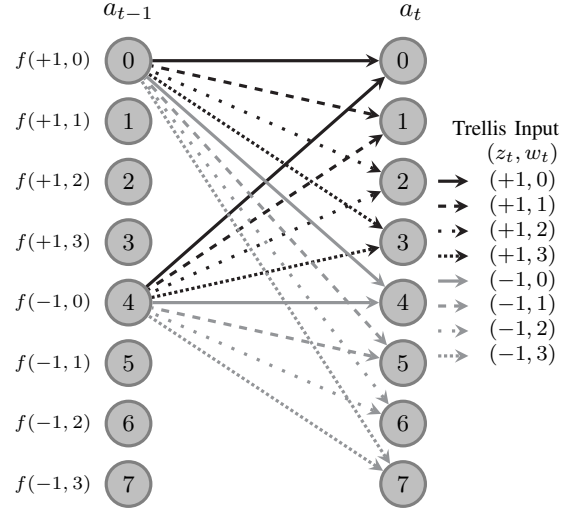


Fig. 5. Trellis section of an impulsive noise detector with a 4-state Markov-Middleton model and DBPSK transmission, showing the auxiliary states defined in (24). For clarity, we only show the state transitions from state-0 and state-4.

This is an essential reference for practical receiver design operating in a specific channel condition. We use a simulation-based method to calculate the AIR between the transmitted sequence \mathbf{z}_1^T and the IN channel output symbols \mathbf{y}_1^T where the input-output relationship is shown in (13). The computation of AIR for channels with memory is explained in detail in [32], and its application to a two-state Markov-Gaussian channel is described in [16]. In this section, we report a detailed AIR analysis for a 4-state Markov-Middleton model with a DBPSK transmission. The algorithm and the computation steps are briefly summarized as follows.

An AIR is the number of information bits that can be reliably transmitted and decoded, with an arbitrarily low error probability per channel used, for a specific modulation format. Specifically, the AIR we consider in this work is the mutual information $I(\mathbf{Z}; \mathbf{Y})$ between the discrete input random process \mathbf{Z} and the continuous output random process \mathbf{Y} , which can be estimated via

$$I(\mathbf{Z}; \mathbf{Y}) \approx \hat{I}(\mathbf{Z}; \mathbf{Y}) = \frac{1}{T} \log p(\mathbf{y}_1^T | \mathbf{z}_1^T) - \frac{1}{T} \log p(\mathbf{y}_1^T) \quad (23)$$

with a very long sequence T . To calculate (23) for channels with memory, [32] introduces a simulation-based computation through a sum-product algorithm with the help of an auxiliary state process. In this paper, we define the auxiliary state realization for a DBPSK transmission over a Markov-Middleton IN channel as

$$a_t = f(z_t \in \mathcal{X}, w_t \in \mathcal{W}) \in \mathcal{A} = \{0, 1, \dots, |\mathcal{A}| - 1\}, \quad (24)$$

where $f : \mathcal{X} \times \mathcal{W} \rightarrow \mathcal{A}$ maps each pair (z_t, w_t) in the product space $\mathcal{X} \times \mathcal{W}$ into a unique state in \mathcal{A} . The size of the auxiliary state space is thus $|\mathcal{A}| = |\mathcal{X}| \times |\mathcal{W}| = 2 \times W$. In Fig. 5, we show an example of the trellis section of the auxiliary state for transmission over a 4-state (i.e., $W = 4$) Markov-Middleton channel.

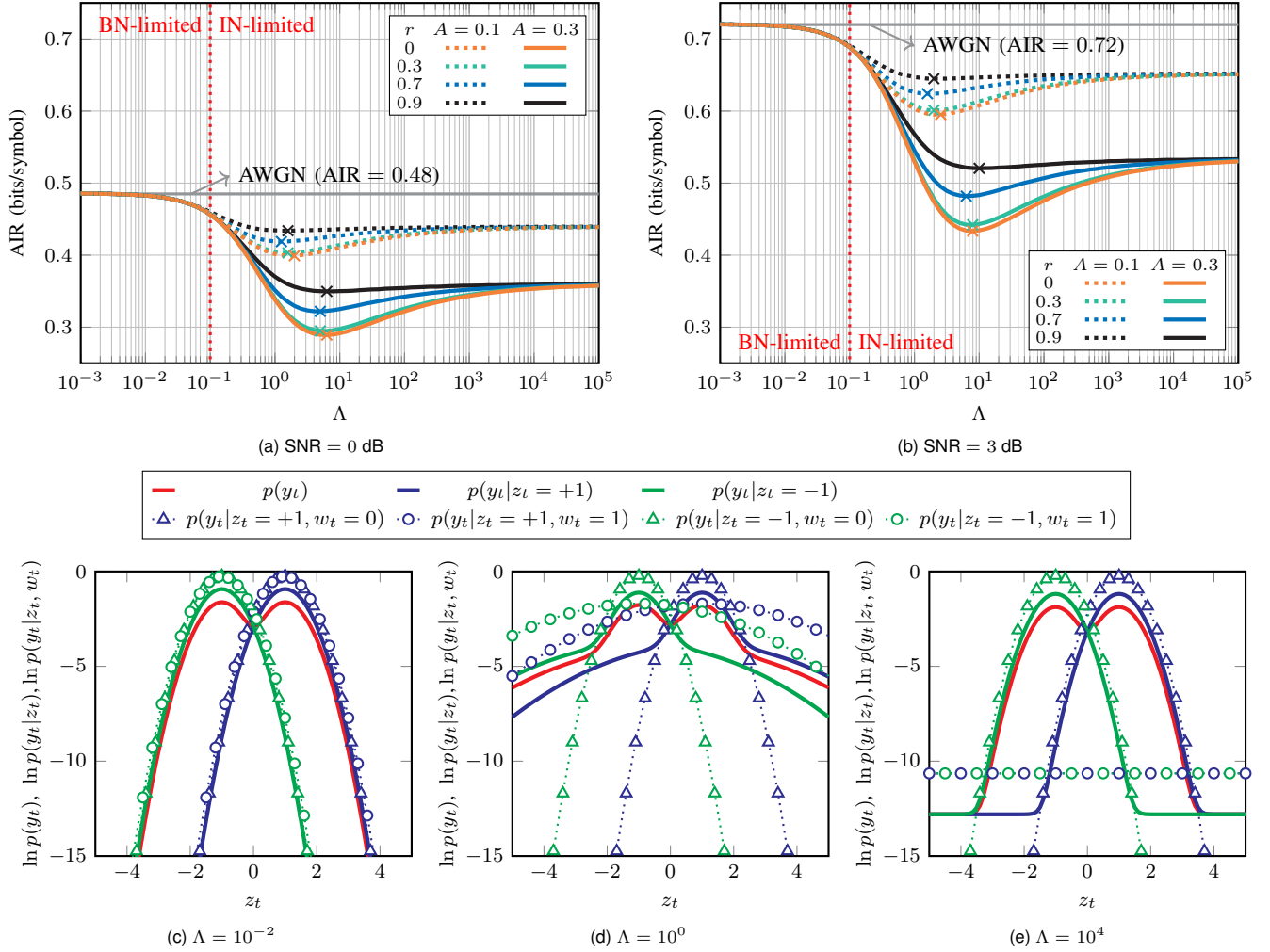


Fig. 6. AIRs versus impulsive-to-background noise ratio Λ for different impulsive index A and correlation parameter r for a DBPSK modulation scheme for a 4-state Markov-Middleton impulsive noise model with (a) SNR = 0 dB and (b) SNR = 3 dB. The crosses denote the minimum AIRs across Λ . The likelihood functions $p(y_t|z_t = +1)$, $p(y_t|z_t = -1)$, $p(y_t|z_t = +1, w_t = 0)$, $p(y_t|z_t = +1, w_t = 1)$, $p(y_t|z_t = -1, w_t = 0)$, and $p(y_t|z_t = -1, w_t = 1)$ of a 2-state memoryless ($r = 0$) Markov-Middleton model are shown for (c) $\Lambda = 10^{-2}$ (d) $\Lambda = 10^0$ and (e) $\Lambda = 10^4$.

The transition probability of the auxiliary states considers the prior transmit symbol probability $p(z_t)$ and the noise state transition matrix defined in (22), which can be expressed as

$$p(a_t|a_{t-1}) = P_{ij} \cdot p(z_t), \quad w_t = j, w_{t-1} = i, \quad (25)$$

The channel likelihood function concerning the auxiliary states (24) can be written as

$$p(y_t|a_t) = \frac{1}{\sqrt{2\pi\sigma_j^2}} \exp\left(-\frac{(y_t - z_t)^2}{2\sigma_j^2}\right), \quad w_t = j. \quad (26)$$

After determining the auxiliary states with their statistical representation (25) and (26), the PDF of the channel output sequence $p(\mathbf{y}_1^T)$ can be calculated via

$$p(\mathbf{y}_1^T) = \sum_{a_T \in \mathcal{A}} p(a_T, \mathbf{y}_1^T) = \sum_{a_T \in \mathcal{A}} \alpha(a_T), \quad (27)$$

using forward recursion (8)–(10), with a branch metric

$$\gamma_a(a_t, a_{t-1}) \triangleq p(y_t|a_t) \cdot p(a_t|a_{t-1}). \quad (28)$$

To compute the PDF of the channel output sequence conditioned on the knowledge of the transmitted symbol sequence $p(\mathbf{y}_1^T|\mathbf{z}_1^T)$, we write

$$p(\mathbf{y}_1^T|\mathbf{z}_1^T) = \frac{p(\mathbf{y}_1^T, \mathbf{z}_1^T)}{p(\mathbf{z}_1^T)} = \frac{\sum_{a_T \in \mathcal{A}} p(a_T, \mathbf{y}_1^T, \mathbf{z}_1^T)}{p(\mathbf{z}_1^T)}. \quad (29)$$

with the help of the auxiliary state. The computation of the joint probability $p(a_T, \mathbf{y}_1^T, \mathbf{z}_1^T)$ can be carried out efficiently using the forward recursion (8)–(10) with a modified branch matrix defined as

$$\gamma_{a,z}(a_t, a_{t-1}) \triangleq p(y_t|a_t) \cdot p(a_t|a_{t-1}, z_t) \cdot p(z_t), \quad (30)$$

where the transition probability conditioned to the knowledge of transmitted symbols is written as

$$p(a_t|a_{t-1}, z_t = \pm 1) = \begin{cases} P_{ij}, & z_t = \pm 1, w_t = j, w_{t-1} = i, \\ 0, & z_t = \mp 1. \end{cases} \quad (31)$$

Given (27) and (29), the estimated AIR, represented by $\hat{I}(\mathbf{Z}; \mathbf{Y})$ can be computed via (23).

In the following analysis, we simulated a sequence of length $T = 10^8$ symbols to compute the estimated AIR, where the transmitted sequence \mathbf{z}_1^T consists of DBPSK modulated symbols produced by (12). The channel output sequence \mathbf{y}_1^T is obtained using (13), where the noise sequence \mathbf{n}_1^T is generated by a 4-state Markov-Middleton model with noise statistics following (18)–(20), given parameters A , Λ , r , and σ_0^2 . The simulated AIR with different Markov-Middleton channel parameters are shown in Figs. 6a–6b for SNRs of 0 dB and 3 dB, respectively. Here, the SNR is defined as the transmitted symbol power over the background noise power

$$\text{SNR} = E\{|z_t|^2\}/\sigma_0^2.$$

To help illustrate the behavior of the AIR over impulsive-to-background noise power ratio Λ , we also plot the likelihood function for a memoryless ($r = 0$) channel with different impulsive-to-background noise power ratios ($\Lambda = 10^{-2}, 10^0, 10^4$) in Figs. 6c–6e. For simplicity, we choose a two-state (background and impulsive states) channel with impulsive index $A = 0.3$ for the likelihood function analysis, which does not affect the generality of the presentation.

Results from Figs. 6a and 6b show that a BN-limited regime can be found when $\Lambda < 10^{-1}$, where the noise generated by an IN state is barely distinguishable from the noise generated by a BN state ($\sigma_0^2 \approx \sigma_j^2$, $j = 1, 2, 3$) as shown in the likelihood function from Fig. 6c. In this case, the performance of the Markov-Middleton channel approaches that of the AWGN channel, with the AIR increasing from 0.48 to 0.72 bits/symbol as the SNR rises from 0 to 3 dB, regardless of the impulsive channel parameters A and r . From Figs. 6a and 6b, we can observe that as Λ increases, the channel transitions into an IN-limited regime, where A and r become crucial in determining the AIR.

Moreover, a non-monotonic behavior of the AIR over Λ is shown in Figs. 6a and 6b, where these exist an inflection point (denoted by crosses), where a minimum AIR occurs. Before the inflection point, the AIR quickly worsens as Λ increases. As shown in Fig. 6d, the IN state increases the uncertainty of the overall likelihood function due to its non-negligible long tail. However, after the inflection point, the impact of the impulsive state on the overall likelihood is reduced. In particular, when $\Lambda > 10^4$, the AIR for all the channels converges to a constant value. This behavior can be explained by examining the likelihood function in Fig. 6e. As the variance of the IN state increases, its likelihood function spreads, and the probability density around the mean decreases compared to that of the BN state. Consequently, the overall likelihood of transmitting a specific symbol $z_t = \pm 1$ is almost entirely dominated by the BN state.

It is also shown in Figs. 6a and 6b that the AIR deteriorates as the IN becomes more pronounced with increasing A . Besides, the inflection point shifts toward large Λ with a higher impulsive index A , which can be explained by (20). Specifically, when the IN samples are more active (larger A), the power of the IN must increase (larger Λ) to maintain the same noise power. On the other hand, the channel memory helps track the noise states through the transition matrix,

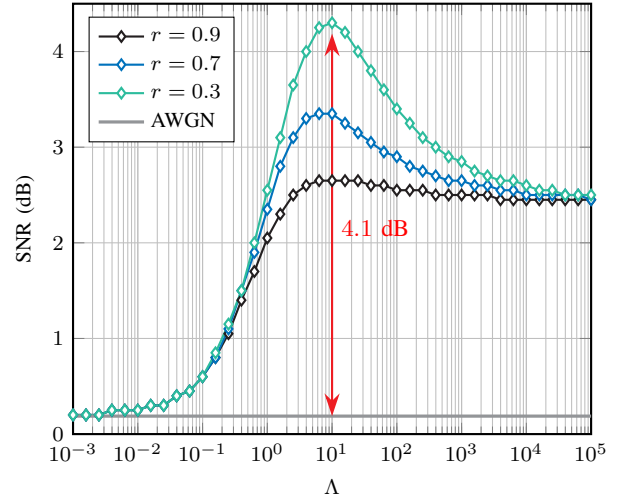


Fig. 7. Required SNR versus impulsive-to-background noise power ratio Λ to achieve 0.5 bits/symbol information rate for a DBPSK modulation scheme under a 4-state Markov-Middleton channel with impulsive index $A = 0.3$.

reducing the uncertainties of the underlying IN channel and thus improving the AIR for any given value of A and Λ .

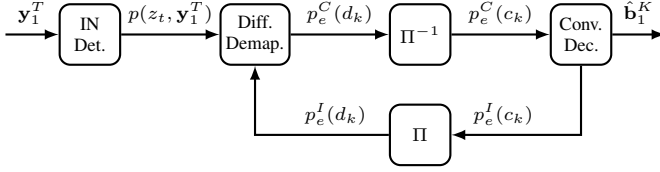
As a reference for our practical receiver design, the required SNR to achieve a target AIR of 0.5 bits per transmitted DBPSK symbol is shown in Fig. 7. We can notice that the Markov-Middleton channel model considered in this work causes large penalties (up to 4.1 dB) compared to an AWGN channel. Note that our results for the Markov-Middleton IN model share similar trends as those in [19] for the memoryless Middleton model and [16] for the Markov-Gaussian model.

V. PRACTICAL RECEIVER DESIGN

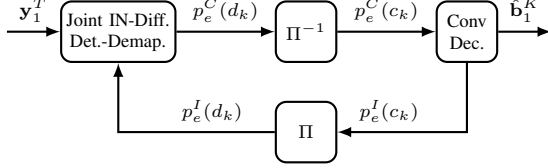
In this section, we propose two practical receiver designs for a bit-interleaved convolutional coded DBPSK transmission that aims at approaching the AIRs calculated in the previous section. Both receivers are designed based on the same transmission format introduced in Sec. III-A and feature a serial turbo-like structure. The main distinction lies in whether the IN detector utilizes the extrinsic prior information provided by the convolutional decoder. The following subsection will commence with a detailed presentation of the separate receiver design, comprising a MAP IN detector and a turbo-DBPSK demapper-decoder system with a block diagram shown in Fig. 8a. Subsequently, we illustrate the joint receiver design in which the IN detector and DBPSK demapper are combined, forming a joint turbo-IN detector-DBPSK demapper-decoder system. The system block diagram for such a joint system design is shown in Fig. 8b.

A. Separate detector and turbo-demapper-decoder receiver

1) *MAP impulsive noise detector*: The states of the IN detector are defined as in (24), and the trellis section is shown in Fig. 5. Given the transition probability (25), likelihood function (26), and the branch metric (28), the joint probability



(a) Separate demapper-detector turbo receiver



(b) Joint demapper-detector turbo receiver

Fig. 8. Block diagrams of (a) the separate detector and turbo-demapper-decoder and (b) the joint turbo-detector-demapper-decoder receiver designs.

$p(a_t, a_{t-1}, \mathbf{y}_1^T)$ of the IN detector is computed via (4)–(11). A MAP-based soft-output detection is then performed through

$$p(z_t, \mathbf{y}_1^T) = \sum_{(a_{t-1} \rightarrow a_t): z_t} p(a_t, a_{t-1}, \mathbf{y}_1^T). \quad (32)$$

where $(a_{t-1} \rightarrow a_t) : z_t$ denotes all the state transitions $(a_{t-1} \rightarrow a_t)$ that is driven by the input symbol z_t .

2) *MAP DBPSK demapper*: The joint probability (32) generated from the IN detector is now used as a soft input, representing the channel information, to the differential symbol demapper. We define the state realization of the differential decoder as

$$p_t = f(z_t \in \mathcal{X}) \in \mathcal{P} = \{0, 1\}, \quad (33)$$

where $f : \mathcal{X} \rightarrow \mathcal{P}$ maps $z_t \in \mathcal{X}$ to a specific state in \mathcal{P} . The trellis section of the DBPSK decoder is shown in Fig. 9. Note that although the state realization p_t is a mapping of the DBPSK symbol z_t , the trellis input is the BPSK modulated symbol x_t , which reveals the structure of the differential encoder in (12).

Using the state definitions (33) and the joint probability $p(z_t, \mathbf{y}_1^T)$ provided the IN detector, we can now rewrite (7) and express the trellis branch metric for the differential decoder as

$$\gamma_p(p_t, p_{t-1}) \triangleq p(z_t, \mathbf{y}_1^T) \cdot p_e^I(x_t), \quad (p_{t-1} \rightarrow p_t) : x_t. \quad (34)$$

where the modified branch metric uses $p(z_t, \mathbf{y}_1^T)$ as the likelihood information and uses the extrinsic prior symbol information $p_e^I(x_t)$ to denote the transition probability $p(p_t|p_{t-1})$ when the state transition $(p_{t-1} \rightarrow p_t)$ is driven by the input symbol x_t . Note that we set $p_e^I(x_t) = p(x_t) = 1/|\mathcal{X}| = 1/2$ in the first iteration. Using the modified branch metric (34), the joint probability of the DBPSK demapper $p(p_t, p_{t-1}, \mathbf{y}_1^T)$ is derived through (4)–(11), and the joint probability of the BPSK symbol is then obtained by

$$p(x_t, \mathbf{y}_1^T) = \sum_{(p_{t-1} \rightarrow p_t): x_t} p(p_t, p_{t-1}, \mathbf{y}_1^T).$$

To perform bit deinterleaving, we need to convert the symbol probability to bit probability as

$$p(d_k, \mathbf{y}_1^T) = \Phi^{-1}[p(x_t, \mathbf{y}_1^T)] \quad (35)$$

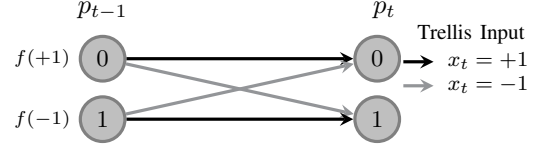


Fig. 9. Trellis section of a DBPSK demapper.

and

$$p_e^I(d_k) = \Phi^{-1}[p_e^I(x_t)],$$

where Φ^{-1} denotes the inverse symbol mapping function that converts the probability of the BPSK symbol x_t back to the probability of the corresponding bit d_k .

3) *Iterative decoding*: One essential part of the turbo decoding principle is to pass only the extrinsic information to each MAP decoder (demapper) block. Extrinsic information refers to the information provided by one decoder (demapper) about one specific bit (symbol), excluding the information directly used to derive it. In other words, it represents new information that can help the other decoder (demapper) refine its estimates. Here, we define the extrinsic likelihood information from the DBPSK demapper as the joint probability $p(d_k, \mathbf{y}_1^T)$ divided by the prior information regarding d_k as

$$p_e^C(d_k) \triangleq \frac{p(d_k, \mathbf{y}_1^T)}{p_e^I(d_k)}.$$

After performing the bit-deinterleaving, we can derive the extrinsic likelihood information of coded bit as

$$p_e^C(c_k) = \Pi^{-1}[p_e^C(d_k)],$$

which is then fed to the convolutional decoder whose state realization is defined as

$$g_k = f(b_k, b_{k-1}, \dots, b_{k-L-1} \in \mathcal{U}^L) \\ \in \mathcal{G} = \{0, 1, \dots, 2^L - 1\},$$

where $f : \mathcal{U}^L \rightarrow \mathcal{G}$ maps \mathcal{U}^L to a distinct states in \mathcal{G} . The modified branch metric for the convolutional decoder is then written as

$$\gamma_g(g_k, g_{k-1}) \triangleq p_e^C(c_k) \cdot p(b_k), \quad (g_{k-1} \rightarrow g_k) : b_k. \quad (36)$$

The extrinsic likelihood information $p_e^C(c_k)$ produced by the DBPSK demapper acts as the convolutional decoder's likelihood information, and $p(b_k) = 1/2$ is the prior bit probability. Again, we compute the joint probability $p(g_k, g_{k-1}, \mathbf{y}_1^T)$ via (4)–(11) using (36) and obtain the joint probability of the information bit as

$$p(b_k, \mathbf{y}_1^T) = \sum_{(g_{k-1} \rightarrow g_k): b_k} p(g_k, g_{k-1}, \mathbf{y}_1^T),$$

and the joint probability of the coded bit as

$$p(c_k, \mathbf{y}_1^T) = \sum_{(g_{k-1} \rightarrow g_k): c_k} p(g_k, g_{k-1}, \mathbf{y}_1^T).$$

To compute the extrinsic prior information produced by the convolutional decoder, we divide the joint probability

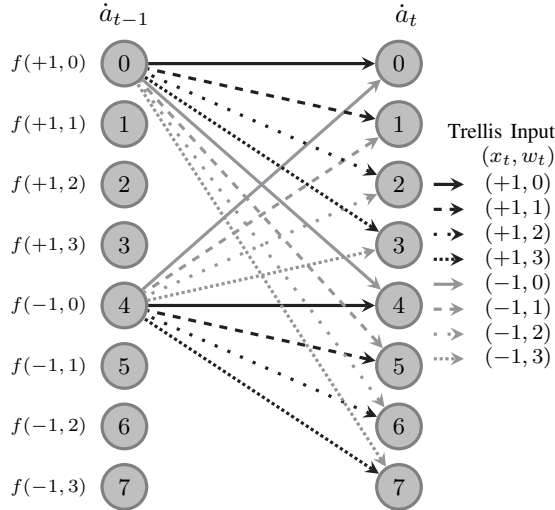


Fig. 10. Trellis section of a joint detector-demapper for a DBPSK transmission and a 4-state impulsive noise. For clarity, we only show the state transitions from state-0 and state-4.

$p(c_k, \mathbf{y}_1^T)$ by the likelihood function $p_e^C(c_k)$ used for deriving it as

$$p_e^I(c_k) \triangleq \frac{p(c_k, \mathbf{y}_1^T)}{p_e^C(c_k)}.$$

After the bit interleaver

$$p_e^I(d_k) = \Pi [p_e^I(c_k)],$$

we can derive the extrinsic prior information of the BPSK symbol via bit-to-symbol mapping

$$p_e^I(x_t) = \Phi[p_e^I(d_k)].$$

The extrinsic symbol information $p_e^I(x_t)$ generated by the convolutional decoder is then fed back as the prior information in (34) of the DBPSK demapper for the next turbo iteration.

B. Joint turbo-detector-demapper-decoder receiver

In the joint detector-demapper design, we construct a super-trellis where the structure of the Markov-Middleton IN detector (Fig. 5) and the DBPSK demapper (Fig. 9) are considered jointly. We define the state realization of the joint super-trellis as \hat{a}_t , which is drawn from the same state space as a_t in (24). However, instead of the differentially encoded symbol z_t , the state transition ($\hat{a}_{t-1} \rightarrow \hat{a}_t$) of the joint detector-demapper is now driven by the BPSK symbol x_t , leading to a transition probability

$$p(\hat{a}_t | \hat{a}_{t-1}) = P_{ij} \cdot p(x_t), \quad w_t = j, w_{t-1} = i. \quad (37)$$

The joint super-trellis section for a DBPSK modulation with a 4-state Markov-Middleton model is shown in Fig. 10. We can now define the branch metric

$$\begin{aligned} \gamma_{\hat{a}}(\hat{a}_t, \hat{a}_{t-1}) &\triangleq p(y_t | \hat{a}_t) \cdot p(\hat{a}_t | \hat{a}_{t-1}) \\ &= p(y_t | a_t) \cdot p(\hat{a}_t | \hat{a}_{t-1}), \end{aligned}$$

TABLE I
NUMBER OF MULTIPLICATIONS FOR SEPARATE AND JOINT TURBO RECEIVER DESIGNS WITH $M = 2$, $W = 4$, AND $L = 2$.

	$I = 0$	$I = 1$	$I = 2$	$I = 3$	$I = 10$
C_{sep}	$168T$	$208T$	$248T$	$288T$	$568T$
C_{jo}	$160T$	$320T$	$480T$	$640T$	$1760T$

compute $p(\hat{a}_t, \hat{a}_{t-1}, \mathbf{y}_1^T)$, and derive the joint symbol probability via the marginalization over all state transitions that are driven by the BPSK symbol x_t as

$$p(x_t, \mathbf{y}_1^T) = \sum_{(\hat{a}_{t-1} \rightarrow \hat{a}_t): x_t} p(\hat{a}_t, \hat{a}_{t-1}, \mathbf{y}_1^T).$$

Subsequently, the iterative processing is the same as in Sec. V-A3.

C. Computational complexity analysis

This subsection offers a general comparison of the complexity between the separate and joint system designs discussed earlier. Since the main computational burden comes from the multiplication operation in the BCJR algorithm, we will concentrate on the complexity related to the number of multiplications used in the BCJR algorithm for two different implementations of turbo systems.

Consider a length T sequence (T trellis sections) processed by a BCJR algorithm with N trellis states. For each state, it needs to consider transitions from all possible previous states, which results in a N^2 multiplication per trellis section. Therefore, the overall complexity of a BCJR operation is given by $2TN^2$, where the constant 2 accounts for the forward and backward operations. For a transmission of a general $M = |\mathcal{X}|$ symbol cardinality and W Markov-Middleton noise states, the separate design in Sec. V-A requires an MW state MAP detector, an M state MAP DPSK demapper, and an M^L state MAP decoder. Considering the turbo receiver is operated over I iterations, we can thus write the computational complexity concerning the number of multiplications of a separate receiver as

$$C_{\text{sep}} = 2T \cdot (M^2W^2 + (I+1)(M^2 + M^{2L})).$$

For a joint design in Sec. V-B, the trellis sections of the IN detector and the DPSK demapper are combined into one super-trellis section with MW state, which results in an overall complexity of

$$C_{\text{jo}} = 2T \cdot (I+1)(M^2W^2 + M^{2L}).$$

In Table I, we show the computational complexity of C_{sep} and C_{jo} for a transmission of a $L = 2$ convolutional code and a DBPSK ($M = 2$) modulation over a 4-state ($W = 4$) Markov Middleton model. When operating without turbo iterations ($I = 0$), the super-trellis design in the joint system has a slightly lower number of multiplications than a separate design. However, as the number of iterations increases, The computational complexity of the joint design increases significantly, nearly doubling the complexity of a separate system design after 2 turbo iterations and tripling after 10 iterations.

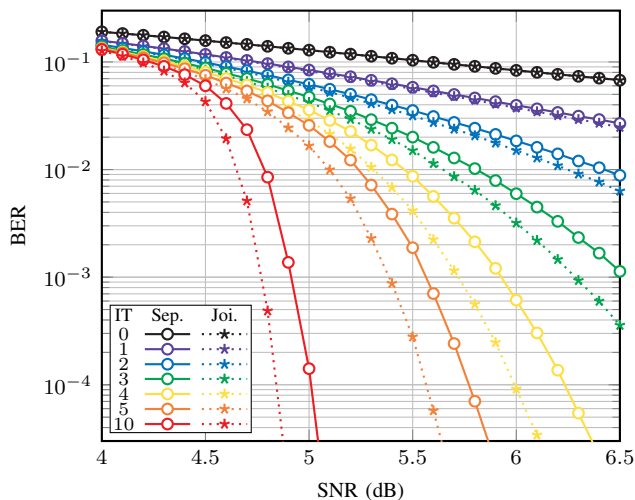


Fig. 11. BER versus SNR of joint and separate turbo DBPSK systems for a 4-state Markov-Middleton impulsive noise channel with parameters $A = 0.3$, $\Lambda = 10$, and $r = 0.7$.

VI. SIMULATION RESULTS

This section reports the numerically simulated bit error rate (BER) performance of the proposed turbo-DBPSK receivers under a 4-state Markov-Middleton IN channel. A standard half-rate convolutional code with generators $(5, 7)_8$ was used. The number of information bits per data frame is 100000, which leads to a bit interleaver with a 200000 bits depth. Such a large interleaver size not only increases the iterative decoding capability but also disperses the bursty impulse noise, which is crucial for the system performance, especially in highly correlated ($r > 0.9$) channels. A BPSK modulation maps the interleaved coded bits to symbols, after which a differential modulator processes the symbols as in (12). Finally, the differentially modulated symbols are transmitted through a Markov-Middleton channel with 4 noise states.

We start by analyzing the BER performance of separate and joint turbo systems with respect to the iteration numbers. The Markov-Middleton model used for the simulation is characterized by $A = 0.3$, $\Lambda = 10$, and $r = 0.7$, corresponding to a highly uncertain channel scenario as indicated by the AIR analysis in Figs. 6a and 6b. As shown in Fig. 11, a joint system consistently outperforms a separate design for all SNRs with a performance gain of around 0.2 dB at a BER of 10^{-4} . This suggests that the system performance is improved by jointly updating the extrinsic information for the combined detector and demapper super trellis. In contrast, in the separate receiver design, the posterior symbol probability of the detector is only calculated once, without iterative updates. In [16], it was reported that the IN detector could barely utilize the soft information produced by the outer decoder, resulting in negligible improvement over iterations. We hypothesize that this is likely due to their results being simulated with a relatively milder IN channel condition characterized by a lower probability of occurrence of the IN state (lower impulsive index).

To further illustrate the system performance under different channel conditions, in Fig. 12, we report the required SNR to

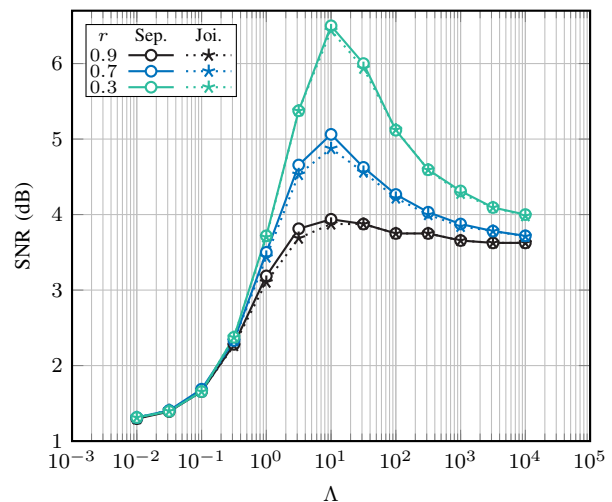


Fig. 12. Required SNR versus impulsive-to-background noise power ratio Λ to achieve 10^{-4} BER for separate and joint turbo-DPSK receiver designs with 10 iterations under a 4-state Markov-Middleton channel with impulsive index $A = 0.3$.

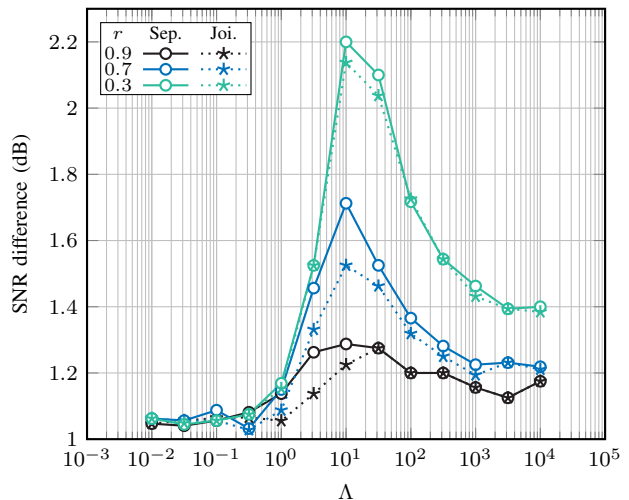


Fig. 13. SNR gap between the AIRs in Fig. 7 and the practical receiver design in Fig. 12 for a DBPSK transmission configuration for a BER request of 10^{-4} .

achieve a BER of 10^{-4} for both separate and joint turbo-DPSK system designs with 10 iterations. The systems were evaluated under the Markov-Middleton channel with a fixed impulsive index $A = 0.3$. The two systems closely follow the estimated AIR behaviors shown in Fig. 7. The joint design of the detector and demapper consistently performs better than or is equal to a separate design. We observe that the performance gain is closely related to the impulsive-to-background noise ratio Λ , with the largest gain approximately at $\Lambda = 10$, corresponding to the most challenging channel condition. In Fig. 13, we demonstrate the SNR gap between the theoretically achievable bound (Fig. 7) and the practical receiver design (Fig. 12) for a DBPSK transmission. We can observe that the performance gap is also dependent on channel conditions. For a small Λ , the proposed receivers can achieve within 1.1 dB from the predicted achievable bound, while in a highly uncertain

channel with correlation parameter $r = 0.3$ and impulsive-to-background noise power ratio $\Lambda = 10$, both receivers have approximately 2.2 dB performance gap from the optimal achievable bound.

VII. CONCLUSIONS

This paper comprehensively evaluates the performance of DBPSK transmission systems under the impairment of a 4-state Markov-Middleton impulse noise model. We started by investigating the AIR between the transmitted sequence and the channel output symbols for various channel conditions. We found that the impulsive index significantly influences the AIR. Also, we observed a non-monotonic relationship between the estimated AIR and the impulsive-to-background noise power ratio, which can be further explained by evaluating the likelihood function for the BN and IN states. Furthermore, channel memory reduces the uncertainty of the given IN channel, thereby increasing the AIR. In the second part of the paper, we proposed two practical turbo-DBPSK receiver structures with a half-rate convolutional code. The first design incorporates a separate IN detector and a turbo-demapper-decoder system. In contrast, the second approach adopts a joint approach, where a turbo-detector-demapper-decoder structure is demonstrated. The joint turbo receiver performs better than a separate one, especially with a large impulsive index A and an impulsive-to-background noise power ratio around $\Lambda = 10^1$. Both proposed joint turbo-DBPSK receiver designs are shown to perform close to the predicted AIR with a gap of approximately 1.1 dB for a moderately IN channel condition.

While a joint system consistently outperforms a separate design, it necessitates greater computational complexity, particularly with a large number of turbo iterations. We have already seen that the joint system can only offer marginal improvements for a channel affected by a slight IN environment. A separate design with lower complexity would be preferable in this situation. However, when dealing with a seriously IN-impacted channel characterized by an impulsive index $A > 0.3$, a joint system may be necessary to enhance the receiver performance. Furthermore, this paper assumes a simple binary modulation format with perfect knowledge of the channel parameters for evaluating the performance of the AIR and the proposed receivers. Extending the systems to higher modulation formats and exploring mismatched decoding scenarios is essential for future research.

ACKNOWLEDGMENT

This work was funded by the RAISE collaboration framework between Eindhoven University of Technology and NXP, including a PPS-supplement from the Dutch Ministry of Economic Affairs and Climate Policy.

REFERENCES

- [1] A. Maouloud, M. Klingler and P. Besnier, "A test setup to assess the impact of EMI produced by on-board electronics on the quality of radio reception in vehicles," *IEEE Trans. Electromagn. Compat.*, vol. 63, no. 6, pp. 1844–1855, Dec. 2021.
- [2] X. Gao, D. Su and Y. Li, "Study on electromagnetic interference of DC/DC converter used in the EV," *Asia-Pacific Symposium on Electromagnetic Compatibility (APEMC)*, pp. 258–261, 2015.
- [3] K. Pliakostathis, "Research on EMI from modern electric vehicles and their recharging systems," *International Symposium on Electromagnetic Compatibility (EMC)*, pp. 1–6, 2020.
- [4] C.-H. Chen, W.-H. Huang, B. Karanov, Y. Wu, A. Young, W. van Houtum, "Analysis of impulsive interference in digital audio broadcasting systems in electric vehicles," *Symposium on Information Theory and Signal Processing in the Benelux (SITB)*, 2024.
- [5] Q. Shan et al., "Noise amplitude distribution of impulsive noise from measurements in a power substation," *International Universities Power Engineering Conference (UPEC)*, pp. 1–5, 2009.
- [6] F. Sacuto, F. Labeau and B. L. Agba, "Wide band time-correlated model for wireless communications under impulsive noise within power substation," *IEEE Trans. Wireless Commun.*, vol. 13, no. 3, pp. 1449–1461, Mar. 2014.
- [7] R. Pighi, M. Franceschini, G. Ferrari and R. Raheli, "Fundamental performance limits for PLC systems impaired by impulse noise," *IEEE International Symposium on Power Line Communications and Its Applications (ISPLC)*, pp. 277–282, 2006.
- [8] M. Zimmermann and K. Dostert, "Analysis and modeling of impulsive noise in broad-band powerline communications," *IEEE Trans. Electromagn. Compat.*, vol. 44, no. 1, pp. 249–258, Feb. 2002.
- [9] W. van Houtum, "Time-division spatial interference rejection (TDSIR)-procedure," U.S. Patent 11,722,197B2, 2022.
- [10] I. Landa, M. M. Véllez, A. Arrinda, R. Torre and M. Fernández, "Impulsive noise characterization and its effect on digital audio quality," *IEEE International Symposium on Broadband Multimedia Systems and Broadcasting (BMSB)*, pp. 1–3, 2015.
- [11] Q. Shan et al., "Estimation of impulsive noise in an electricity substation," *IEEE Trans. Electromagn. Compat.*, vol. 53, no. 3, pp. 653–663, Aug. 2011.
- [12] S. A. Bhatti, I. A. Glover, R. Atkinson, Q. Shan, Y. Yang, J. M. R. S. Neto, "Vulnerability of bluetooth to impulsive noise in electricity transmission substations," *IET International Conference on Wireless Sensor Network (WSN)*, pp. 53–58, 2010.
- [13] N. B. Sarr, A. K. Yazbek, H. Boeglen, J. P. Cances, R. Vauzelle and F. Gagnon, "An impulsive noise resistant physical layer for smart grid communications," *IEEE International Conference on Communications (ICC)*, pp. 1–7, 2017.
- [14] D. Middleton, "Statistical-physical model of electromagnetic interference," *IEEE Trans. Electromagn. Compat.*, vol. EMC-19, no. 3, pt. 1, pp. 106–127, Aug. 1977.
- [15] D. Middleton, "Non-Gaussian noise models in signal processing for telecommunications: new methods and results for class A and class B noise models," *IEEE Trans. Inf. Theory*, vol. 45, no. 4, pp. 1129–1149, May 1999.
- [16] D. Fertonani and G. Colavolpe, "On reliable communications over channels impaired by bursty impulse noise," *IEEE Trans. Commun.*, vol. 57, no. 7, pp. 2024–2030, Jul. 2009.
- [17] G. Ndo, F. Labeau and M. Kassouf, "A Markov-Middleton model for bursty impulsive noise: Modeling and receiver design," *IEEE Trans. Power Del.*, vol. 28, no. 4, pp. 2317–2325, Oct. 2013.
- [18] R. Haring and A. J. Han Vinck, "Performance bounds for optimum and suboptimum reception under Class-A impulsive noise," *IEEE Trans. Commun.*, vol. 50, no. 7, pp. 1130–1136, Jul. 2002.
- [19] D. Fertonani and G. Colavolpe, "Theoretical limits and practical detection schemes for channels affected by class-A impulse noise," *IEEE Global Telecommunications Conference (GLOBECOM)*, pp. 146–150, 2007.
- [20] D. Fertonani and G. Colavolpe, "A robust metric for soft-output detection in the presence of class-A noise," *IEEE Trans. Commun.*, vol. 57, no. 1, pp. 36–40, Jan. 2009.
- [21] J. Mitra and L. Lampe, "Convolutionally coded transmission over Markov-Gaussian channels: analysis and decoding metrics," *IEEE Trans. Commun.*, vol. 58, no. 7, pp. 1939–1949, Jul. 2010.
- [22] F. G. Mengistu, D. -F. Tseng, Y. S. Han, M. A. Mulatu and L.-C. Chang, "A Robust decoding scheme for convolutionally coded transmission through a Markov Gaussian channel," *IEEE Trans. Veh. Technol.*, vol. 63, no. 9, pp. 4344–4356, Nov. 2014.
- [23] D.-F. Tseng, F. G. Mengistu, Y. S. Han, M. Abera Mulatu, L.-C. Chang and T. -R. Tsai, "Robust turbo decoding in a Markov Gaussian channel," *IEEE Wireless Commun. Lett.*, vol. 3, no. 6, pp. 633–636, Dec. 2014.
- [24] M. S. Alam, B. Selim, G. Kaddoum and B. L. Agba, "Mitigation techniques for impulsive noise with memory modeled by a two state Markov-Gaussian process," *IEEE Syst. J.*, vol. 14, no. 3, pp. 4079–4088, Sep. 2020.

- [25] H. Nakagawa, D. Umehara, S. Denno and Y. Morihoro, "A decoding for low density parity check codes over impulsive noise channels," *International Symposium on Power Line Communications and Its Applications (ISPLC)*, pp. 85–89, 2005.
- [26] D. Umehara, H. Yamaguchi and Y. Morihoro, "Turbo decoding in impulsive noise environment," *IEEE Global Telecommunications Conference (GLOBECOM)*, pp. 194–198, 2004.
- [27] G. Colavolpe, "Classical coherent receivers for differentially encoded M-PSK are optimal," *IEEE Commun. Lett.*, vol. 8, no. 4, pp. 211–213, Apr. 2004.
- [28] K. R. Narayanan and G. L. Stuber, "A serial concatenation approach to iterative demodulation and decoding," *IEEE Trans. Commun.*, vol. 47, no. 7, pp. 956–961, Jul. 1999.
- [29] P. Hoeher and J. Lodge, "Turbo DPSK: iterative differential PSK demodulation and channel decoding," *IEEE Trans. Commun.*, vol. 47, no. 6, pp. 837–843, Jun. 1999.
- [30] W. van Houtum, "Two-dimensional block-based reception for differentially encoded OFDM systems: A study on improved reception techniques for digital audio broadcasting systems," Ph.D. dissertation, Dept. Elect. Eng., Technische Universiteit Eindhoven, Eindhoven, Netherlands, 2012.
- [31] I. Lee, "The effect of a precoder on serially concatenated coding systems with an ISI channel," *IEEE Trans. Commun.*, vol. 49, no. 7, pp. 1168–1175, Jul. 2001.
- [32] D. M. Arnold, H.-A. Loeliger, P. O. Vontobel, A. Kavcic and W. Zeng, "Simulation-based computation of information rates for channels with memory," *IEEE Trans. Inform. Theory*, vol. 52, no. 8, pp. 3498–3508, Aug. 2006.
- [33] L. R. Bahl, J. Cocke, F. Jelinek, and J. Raviv, "Optimal decoding of linear codes for minimizing symbol error rate," *IEEE Trans. Inform. Theory*, vol. 20, no. 2, pp. 284–287, Mar. 1974.